Pharmaceutical Sciences Asia

Pharm Sci Asia 2026; 53(4), 556-566

DOI:10.29090/psa.2026.04.26.11335

Research Article

Uncaria gambir extract nanoparticles inhibit lung fibrosis progression in a bleomycin-induced rat model: A histopathological study

Lukman N Rahman[1], Gondo Mastutik[2]*, Anny S Rahaju[2], Dyah Fauziah[2], Nanik S Aminah[3,4], Aditya S Sari[2], Heru F Trianto[5].

[1] Master Program of Basic Medical Sciences, Faculty of Medicine, Universitas Airlangga, Surabaya, East Java, Indonesia, 60132.
[2] Department of Anatomical Pathology, Faculty of Medicine, Universitas Airlangga, Surabaya, East Java, Indonesia, 60132
[3] Department of Chemistry, Faculty of Science and Technology, Universitas Airlangga, Surabaya, East Java, Indonesia
[4] Biotechnology of Tropical Medicinal Plants Research Group, Universitas Airlangga, Surabaya, East Java, Indonesia
[5] Department of Anatomical Pathology, Faculty of Medicine, Universitas Tanjungpura, Pontianak, Indonesia

ABSTRACT

Pulmonary fibrosis (PF) is characterized by the thickening of alveolar walls due to excessive accumulation of fibrotic tissue within various lung structures, ultimately leading to progressive respiratory failure and mortality. Current therapeutic options for PF are limited and primarily aim to slow disease progression. These drugs have significant limitations, including adverse effects and lack of survival benefit. *Uncaria gambir* Roxb. has demonstrated antifibrotic effects through NF-κB and TGF-*β* signaling pathways. Nanoparticle delivery systems improve stability and controlled release. This study aimed to evaluate the antifibrotic effects of *Uncaria gambir* extract nanoparticles (G-NPs) through histopathological assessment. Twenty-five Wistar rats were randomly allocated into five groups (n = 5 per group): two groups as control and treatment groups receiving G-NPs (50, 100, and 200 mg/kg body weight (BW)). Bleomycin (1.5 mg/kg) was administered intratracheally on day 0 to induce PF. All parameters were assessed using digital pathology with slide imaging and analyzed using QuPath® software. Treatment with G-NPs at a dose of 200mg/kg BW exhibited the most pronounced therapeutic effect, reducing the percentage of lung injury, lung injury score, interalveolar septal thickness, percentage of collagen deposition in lung tissue, and Ashcroft score. These improvements were significantly enhanced relative to the 50 and 100 mg/kg BW doses ($p < 0.001$). Treatment with G-NPs (200 mg/kg BW) demonstrated the greatest histological improvement in reducing the progression of lung fibrosis, indicating the antifibrotic potential of G-NPs.

Keywords:
Chronic respiratory diseases; Histopathology; Pulmonary fibrosis; *Uncaria gambir*

1. INTRODUCTION

Pulmonary fibrosis (PF) is characterized by the thickening of alveolar walls due to excessive accumulation of fibrotic tissue within various lung structures, ultimately leading to progressive respiratory failure and mortality[1,2]. Fibrotic lung diseases encompass a range of conditions in humans, among which idiopathic pulmonary fibrosis (IPF) is the most prevalent[3,4], and its prevalence has increased globally in recent years[5]. IPF is associated with poor prognosis. The average survival rate is approximately 3 - 5 years following diagnosis[6]. The disease results from repetitive alveolar epithelial injury and dysregulated wound healing processes[3]. The mechanisms contribute to its pathogenesis, including the PI3K/Akt/mTOR and WNT/β-catenin pathways, with the TGF-β/Smad signaling pathway playing the most prominent role[5,6].

***Corresponding author:**
* Gondo Mastutik Email: gondomastutik@fk.unair.ac.id

Pharmaceutical Sciences Asia © 2026 by
Faculty of Pharmacy, Mahidol University, Thailand is licensed under CC BY-NC-ND 4.0. To view a copy of this license, visit
https:// www.creativecommons.org/licenses/by-nc-nd/4.0/

Current therapeutic options for IPF limited and primarily aim to slow disease progression. To date, pirfenidone and nintedanib have been approved by the FDA[6–8]. However, these drugs have significant limitations, including adverse effects and lack of survival benefit[6]. Therefore, there is an urgent need to identify novel, safe, and effective therapeutic compounds[7]. The bleomycin-induced model closely mimics human pulmonary fibrosis[5,7]. Histopathological analysis using semiquantitative scoring systems remains the gold standard, while digital whole-slide image analysis reduces subjectivity and provides continuous quantitative data[2,7,9].

Uncaria gambir Roxb., which is classified within the family Rubiaceae, contains flavonoids, alkaloids, tannins, terpenoids, and saponins, with catechins comprising 40–80% of the dry extract[10,11]. It has demonstrated antifibrotic effects through NF-κB and TGF-β signaling pathways[10–12]. However, catechin have low oral bioavailability (<5%) and limited absorption[6,13,14]. Nanoparticle delivery systems improve stability and controlled release[15]. Sodium alginate–based nanoparticles (78.40 ± 12.25 nm) of *Uncaria gambir* extract at doses of 50–200 mg/kg, enhancing stability and release[16]. Therefore, this study aimed to evaluate the antifibrotic effects of *Uncaria gambir* extract nanoparticles (G-NPs) through histopathological assessment using digital pathology image analysis integrated deep learning-based image analysis.

2. MATERIALS AND METHODS

2.1. Plant, drugs and chemicals materials

Materials used for G-NPs extract preparation included powdered *U. gambir* sap processed into an ethyl acetate extract, sodium alginate as the nanoencapsulation material, and methanol, n-hexane, and ethyl acetate as solvents for extraction and fractionation[16]. Additional materials included 0.9% normal saline; bleomycin HCl (Nippon Kayaku Kabushiki Kaisha®, Japan) as the fibrosis-inducing agent; distilled water; standard laboratory rat feed (Pokphand, Indonesia); water (PAM, Indonesia); and 10% formalin for fixation. Histopathology utilized graded alcohol series, acid alcohol, xylol, Harris's hematoxylin, alcoholic eosin, ammonia, Entellan mounting medium, Mayer's egg albumin, and Masson's trichrome staining.

2.2. Preparation of nanoparticle

Uncaria gambir extract was obtained through extraction, fractionation, and isolation, and was subsequently nanoencapsulated using sodium alginate (Na-alginate) following a previously reported method[16]. The G-NPs were characterized in terms of particle size, polydispersity index (PDI), zeta potential, loading efficiency (LE), loading amount (LA), morphology, and stability. The particle size was 78.40 ± 12.25 nm, with a PDI of 0.55 ± 0.01 and a zeta potential of −40.87 ± 0.90 mV. The loading efficiency and loading amount were 97.56 ± 0.04% and 32.52 ± 0.01%, respectively. The G-NPs exhibited a spherical morphology, as characterized by Atomic Force Microscopy (AFM), rather than SEM or TEM, with an AFM particle size of approximately 70 nm. Regarding stability, G-NPs maintained stable UV–Vis absorption at pH 3–11, whereas a spectral change was observed at pH 12. Temperature stability was evaluated at 30–100°C, while ionic stability was assessed at NaCl concentrations of 0–0.30 M[16].

2.3. Preparation of animals and induction of pulmonary fibrosis

This was a true experimental study with a post-test control group design. In this study, the sample size was determined using the Federer formula (1991), which is used for experimental research with several treatment groups. The formula used is: $(t - 1)(n - 1) \geq 15$, where t is the number of treatment groups and n is the number of animals in each group. This study consisted of five groups; therefore the sample size calculation was: $(5 - 1)(n - 1) \geq 15$ $4(n - 1) \geq 15$ $4n - 4 \geq 15$ $4n \geq 19$ $n \geq 4.75$. Thus, the minimum sample size required was 5 mice per group. Based on these calculations, 5 mice were used in each group; therefore the minimum number of animals required was 25.

Twenty-five rats (*Rattus norvegicus*), male, aged 8 - 10 weeks and weighing 150 - 250 g, were acclimatized for 7 days under controlled laboratory conditions, maintained on a 12-hour light and dark cycle and provided ad libitum access to food and water. After the adaptation period was completed, the mice were randomly allocated into five research cage groups (n = 5 per cage): three treatment groups receiving G-NPs (50, 100, and 200 mg/kg body weight (BW)), and two control groups designated as negative control (receiving normal saline) and positive control (receiving Bleomycin) to minimize stress and the risk of fighting due to cage transfer. The doses of 50, 100, and 200 mg/kgBW in this study were based on the research stage of Wardana et al[16] in the series of G-NP development[16]. On day 0, the negative control group received saline, while others were administered bleomycin via intratracheal instillation. From day 9–23, the treatments were administered once daily via orogastric gavage.

Bleomycin hydrochloride (1.5 mg/kg) was prepared and diluted in 500 µL normal saline, according to previous protocols[17]. The rats were anesthetized with xylazine (5 mg/kg) and 10% ketamine (50–100 mg/kg)

before intratracheal instillation. The animals were positioned vertically in an acrylic fixation device to facilitate tracheal visualization using a portable otoscope. A 22G intravenous catheter was inserted into the trachea, and bleomycin was injected.

2.4. Histopathological examination

After 14 days of treatment, the animals were euthanized on day 23. Lung tissues were harvested, fixed in 10% buffered formalin, and processed according to standard histopathological preparation protocols. The evaluated parameters included the percentage of lung injury, interalveolar septal thickness, pulmonary fibrosis score based on the modified Ashcroft scale, and percentage of collagen deposition in lung tissue. Microscopic examination was performed using an microscope (Olympus CX23, Tokyo, Japan) at 100× magnification. Measurements were expressed as mean (± SD) from 15 randomly selected fields per lung lobe (five lobes per rat) and were analyzed using QuPath® software[18,19].

Interalveolar septal thickness and degree of lung injury were evaluated using slides stained with hematoxylin and eosin (H&E). The degree of lung injury was assessed using a semi-quantitative scoring system based on the evaluation of edema, hemorrhage, inflammation, and atelectasis. Each parameter was graded on a scale of 0–4 as follows: no injury = 0; injury involving 25% of the field = 1; 50% = 2; 75% = 3; and 100% of the field = 4[20].

Fibrosis was evaluated using Masson's Trichrome staining with the modified Ashcroft scale, and comparisons were made to the control group. Representative grading criteria (0–8) (Figure 1)[21]. The collagen percentage was defined as the ratio of the collagen-positive region to the overall lung tissue area. Histopathological image analysis was performed

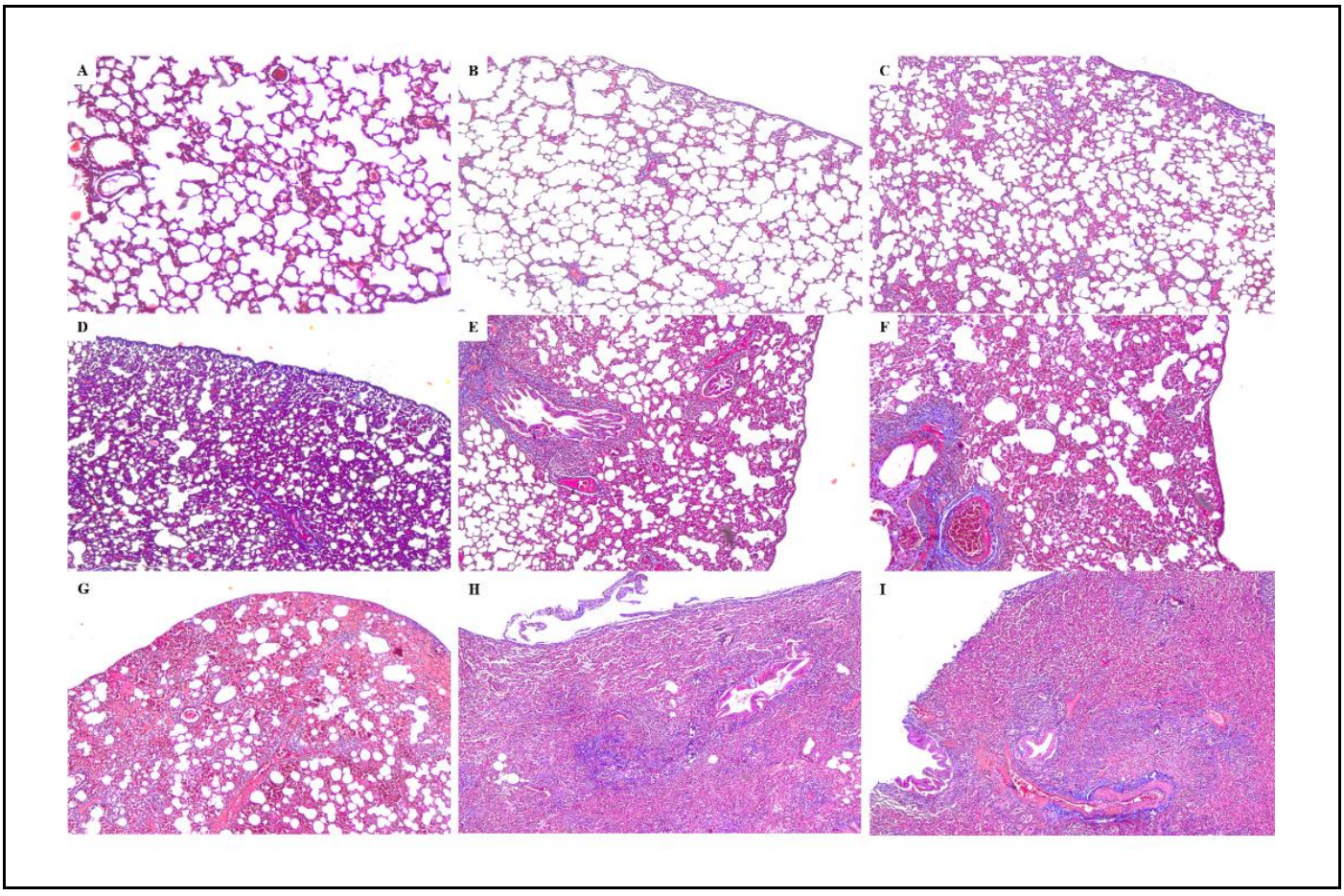


Figure 1. Assessment of lung fibrosis using the modified Ashcroft scale in Masson's Trichrome staining. (A) Grade 0: normal lung architecture. (B) Grade 1: isolated thickening of alveolar septa (septum ≤3× thicker than normal) with mild fibrotic changes. (C) Grade 2: fibrotic thickening of alveolar septa (septum >3× thicker than normal) with focal nodular (knot-like) formations. (D) Grade 3: continuous fibrotic thickening of alveolar septa (septum >3× thicker than normal). (E) Grade 4: heterogeneous alveolar septa with discrete fibrotic masses (≤10% of the microscopic field). (F) Grade 5: confluent fibrotic masses involving >10% to ≤50% of the microscopic field; lung architecture is severely distorted but partially preserved, with variable alveolar septa. (G) Grade 6: large contiguous fibrotic masses (>50% of the microscopic field); lung architecture mostly not preserved, and alveolar septa variable or mostly absent. (H) Grade 7: absence of alveolar septa; alveolar architecture is nearly obliterated by fibrotic masses, with up to five residual air spaces remaining. (I) Grade 8: complete loss of alveolar septa; microscopic field completely obliterated with fibrotic masses.

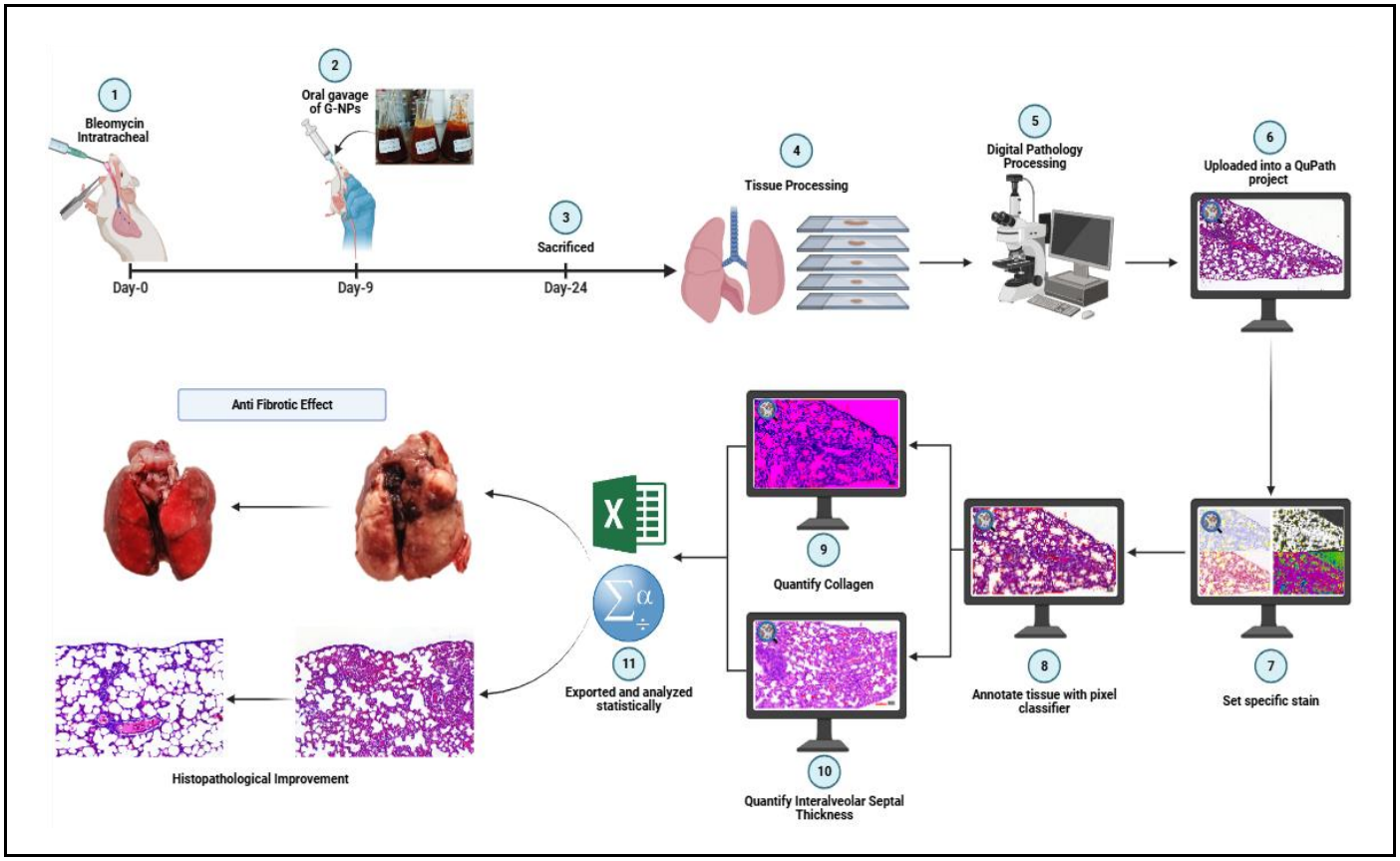


Figure 2. Experimental and analytical workflow for assessing the antifibrotic effects of *Uncaria gambir* extract nanoparticles (G-NPs). (1) A pulmonary fibrosis model was induced by bleomycin hydrochloride at a dose of 1.5 mg/kg body weight (BW), dissolved in 500 µL, intratracheally on day 0. (2) G-NPs were administered daily from day 9 to day 23 (50, 100, and 200 mg/kg BW). (3) On day 24, the animals were euthanized, and lung tissues were collected. (4) The lung samples were processed into five histological slides representing each lobe (right lung: superior, medial, inferior, and postcaval lobes; left lung: single lobe). (5) Digital images of all histological slides were captured using a microscope camera integrated with Leica Enersight software. (6) The resulting slide images were uploaded to a QuPath project. (7) The appropriate staining settings were configured according to the analytical requirements. (8) The lung tissue sections were annotated using a pixel classifier to (9) quantify the collagen area percentage and (10) measure interalveolar septal thickness, defined as the linear distance between opposing alveolar surfaces (µm). (11) The quantitative data were exported to Microsoft Excel and subsequently analyzed statistically using SPSS version 27. (12) Histopathological improvement. Created with BioRender.com.

using QuPath software (Figure 2). The analysis stages began with opening and calibrating the histopathological image according to the microscope scale used. Next, the region of interest (ROI) was determined in the tissue area to be analyzed using the Simple Tissue Detection feature. For staining quantification, pixel classification was performed using the Classify feature, followed by Pixel Classification. The pixel classifier was created based on the staining characteristics of the analyzed tissue and was saved with a name corresponding to the type of staining, for example, Masson's Trichrome. The created classifier was then applied to the previously determined ROI by selecting the classifier from the Choose model menu and running the Measure function. The classification results were used to determine the proportion of the tissue area that showed the target staining. Quantification was expressed as the percentage of the stained tissue area to the total tissue area in the ROI (% stained area/total tissue area). Septal thickness was defined as the wall separating adjacent alveoli and was measured as the linear distance between opposing alveolar surfaces using a perpendicular line tool and expressed in micrometers (µm). Measurements were conducted on the same ROI for the entire research group with a consistent analysis procedure. The measurement results were then displayed in the Measurements section of QuPath. The measurement data were exported in.tsv format through the Measurements feature, then Export measurements, and subsequently used for statistical analysis., and the results were expressed as a percentage[22,23].

2.5. Statistical analysis

Data normality was evaluated using the Shapiro–Wilk test. For parametric data, one-way ANOVA followed by Tukey's multiple comparison post hoc test was employed, whereas the Kruskal–Wallis test with Mann–Whitney U or Bonferroni post hoc testing was used for non-parametric data and considered significant at $p < 0.05$.

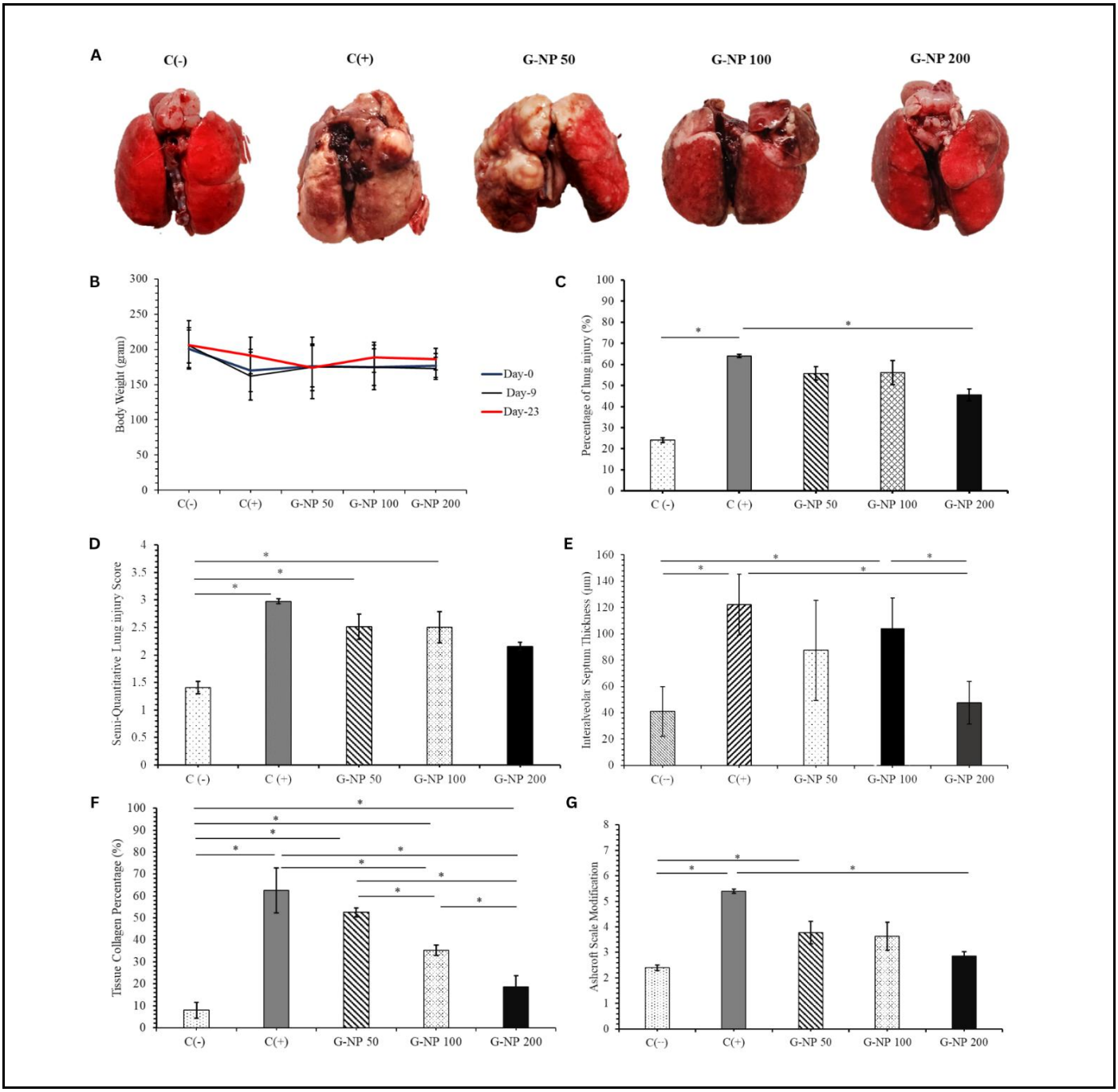


Figure 3. Evaluation of Macroscopic Morphology, Body Weight, and Lung Histopathological Parameters. Macroscopic morphology (A), body weight (B), Percentage of lung injury (C), Semi-quantitative lung injury score (D), Alveolar septal thickness (E), Percentage of lung tissue collagen (F), and Ashcroft score (G). Note: C(–): Negative control group. C(+): Positive control group. G-NPs 50, 100, 200: Nano *Uncaria gambir* at 50, 100, 200 mg/kg BW, respectively. *p-value < 0.05.

3. RESULTS

3.1. Macroscopic characteristics and body weight

The macroscopic appearance of the lungs from the bleomycin-induced groups treated with G-NPs (Figure 3A). In the normal control group receiving normal saline, the lungs appeared uniformly bright red with a smooth surface, without visible nodules or discoloration, reflecting preserved tissue architecture. In contrast, the bleomycin-induced group exhibited marked alterations, including paler-to-brownish discoloration, irregular surface contours, nodular formations, tissue thickening, and increased consistency. Some regions also displayed dark patches suggestive of hemorrhage or fibrotic deposition. Treatment with G-NPs at a dose of 50 mg/kg showed partial improvement, whereas 100 mg/kg demonstrated greater recovery. Notably, treatment with 200 mg/kg produced lung morphology that most closely resembled that of the normal control group.

Body weight (BW) was analyzed on days 0, 9, and 23 using repeated-measures ANOVA (Figure 3B). No statistically significant changes in BW were observed over time within each group ($p > 0.05$). The negative control group showed gradual weight gain, while the positive control group experienced weight loss on day 9, followed by partial recovery on day 23. The G-NPs treatment groups (50, 100, and 200 mg/kg) exhibited relatively stable BW, with slight increases at the end of observation, without significant differences compared to controls.

3.2. Lung injury

Analysis showed significant differences in the percentage of lung injuries between the groups ($p < 0.001$). Bonferroni-adjusted pairwise comparisons showed a significant difference between the negative and positive control groups (adjusted $p < 0.001$). The G-NPs 200 mg/kg BW group also differed significantly from the positive control (adjusted $p = 0.010$). However, no significant differences were observed between the G-NPs 50, 100, and 200 mg/kg BW groups (adjusted $p > 0.05$) (Figure 3C). The semi-quantitative ALI scores differed significantly among the treatment groups ($p < 0.001$). Bonferroni-adjusted pairwise comparisons showed significant differences between the negative control group and the G-NPs 50 mg/kg BW, 100 mg/kg BW, and positive control groups (adjusted $p = 0.002$ for each comparison). However, no significant differences were observed between the negative control and G-NPs 200 mg/kg BW (adjusted $p = 1.000$), or among the G-NPs 200 mg/kg BW with 50 mg/kg BW, 100 mg/kg BW, and positive control groups (adjusted $p > 0.05$) (Figure 3D).

Histopathological examination revealed that the bleomycin-induced group exhibited marked alveolar structural damage, characterized by thickened alveolar septa, vascular congestion, mononuclear inflammatory cell infiltration, and dense extracellular matrix deposition. In contrast, the normal saline group showed preserved alveolar architecture with thin interalveolar septa and wide alveolar spaces without inflammatory infiltration. Treatment with G-NPs (50, 100, and 200 mg/kg BW) demonstrated progressive histopathological improvement, including thinner septa, reduced inflammatory cell infiltration, and more open alveolar spaces compared with the bleomycin-induced group (Figure 4).

3.3. Interalveolar septal thickness

According to the findings of the One-Way ANOVA, we observed a significant difference in the mean alveolar septum thickness (μm) among the five treatment groups ($p < 0.001$), indicating that at least one group had a septum thickness that was significantly different from the others. The results of the Tukey HSD post hoc test showed that the negative control group had a significantly lower septum thickness than the positive control (mean difference = −81.22 μm; $p < 0.001$) and G-NPs 100 mg/kg BW (mean difference = −63.39 μm; $p = 0.005$). Meanwhile, the difference between the negative control and G-NPs 50 mg/kg BW was not significant ($p = 0.055$), nor was the difference between the negative control and G-NPs 200 mg/kg BW ($p = 0.993$). The positive control group showed a significantly higher septum thickness than G-NPs 200 mg/kg BW (mean difference = 74.54 μm; $p = 0.001$). However, there was no significant difference between the positive control and G-NPs 50 mg/kg BW ($p = 0.220$) or G-NPs 100 mg/kg BW ($p = 0.789$).

Furthermore, the G-NPs 100 mg/kg BW group had a significantly higher septum thickness than the G-NPs 200 mg/kg BW group (mean difference = 56.71 μm; $p = 0.014$). There was no significant difference between the G-NPs 50 mg/kg BW and G-NPs 100 mg/kg BW groups ($p = 0.819$) or between the G-NPs 50 mg/kg BW and G-NPs 200 mg/kg BW groups ($p = 0.126$) (Figure 3E).

3.4. Lung tissue collagen percentage

According to the findings of the One-Way ANOVA, there was a highly significant difference in collagen content (%) among the five research groups ($p < 0.001$). The Tukey HSD post hoc test showed that the negative control group had a significantly lower collagen content compared to the positive control (mean difference = −54.51%; $p < 0.001$), as well as the groups receiving G-NPs 50 mg/kg BW (−44.59%; $p < 0.001$), G-NPs 100 mg/kg BW (−27.34%; $p < 0.001$), and G-NPs 200 mg/kg BW (−10.57%; $p = 0.048$) Compared to the positive control, the G-NPs 50 mg/kg BW group did not show a significant difference (mean difference = 9.92%; $p = 0.070$). However, the positive control had a collagen content that was significantly higher than the G-NPs 100 mg/kg BW group (27.17%; $p < 0.001$) and the G-NPs 200 mg/kg BW group (43.94%; $p < 0.001$).

Among the G-NPs administration groups, there were significant differences between G-NPs 50 and G-NPs 100 mg/kg BW (17.25%; $p = 0.001$), as well as between G-NPs 50 and G-NPs 200 mg/kg BW (34.02%; $p < 0.001$). Additionally, the G-NPs 100 mg/kg BW group had a collagen content that was significantly higher than that of the G-NPs 200 mg/kg BW group (16.77%; $p = 0.001$) (Figure 3F).

3.5. Degree of fibrosis

The findings of the analysis conducted using the Kruskal-Wallis test showed significant differences

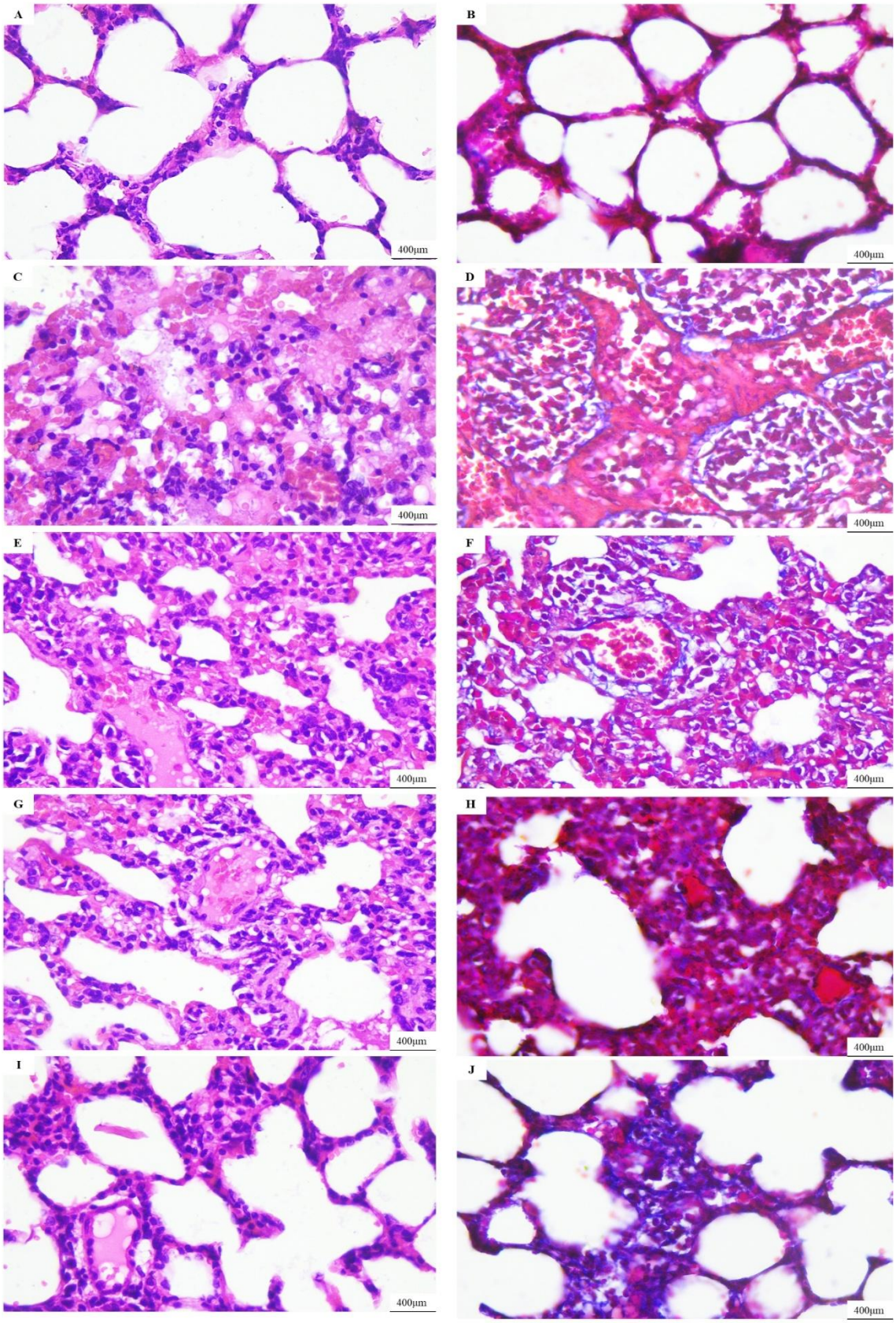


Figure 4. Histopathological characteristics of lung tissue. Panels A, C, E, G, and I show H&E staining, while panels B, D, F, H, and J show Masson's Trichrome staining (400 µm magnification). The groups include the negative control (A, B), positive control (C, D), and Nano *Uncaria gambir*–treated groups at doses of 50 mg/kg body weight (E, F), 100 mg/kg body weight (G, H), and 200 mg/kg body weight (I, J).

in the Ashcroft Scale scores among the treatment groups ($p < 0.001$). These results indicate that the level of pulmonary fibrosis differed significantly among the five research groups. Pairwise comparison analysis conducted with Bonferroni correction showed that the negative control group had a significant difference in Ashcroft Scale scores compared to the G-NPs 50 mg/kg BW group (adjusted $p = 0.043$) and the positive control group (adjusted $p < 0.001$). Meanwhile, there was no significant difference between negative control group and G-NPs 200 mg/kg BW (adjusted $p = 1.000$) or between negative control group and G-NPs 100 mg/kg BW (adjusted $p = 0.119$).

Among the treatment groups, no significant differences were found between G-NPs 200 mg/kg BW and G-NPs 100 mg/kg BW (adjusted $p = 1.000$), nor between G-NPs 200 mg/kg BW and G-NPs 50 mg/kg BW (adjusted $p = 0.745$). However, a significant difference was observed between G-NPs 200 mg/kg BW and the positive control group (adjusted $p = 0.013$). No significant differences were found between G-NPs 100 mg/kg BW and G-NPs 50 mg/kg BW (adjusted $p = 1.000$), G-NPs 100 mg/kg BW and positive control group (adjusted $p = 0.745$), or G-NPs 50 mg/kg BW and positive control group (adjusted $p = 1.000$) (Figure 3G).

4. DISCUSSION

Bleomycin-induced pulmonary fibrosis recapitulates the clinical and pathological spectrum observed in human pulmonary fibrosis. Bleomycin induces pneumonitis and fibrosis, initially characterized by acute inflammation involving alveolar epithelial injury, inflammatory cell infiltration, and mediator release, followed by fibroblast proliferation and extracellular matrix deposition. ROS generation leads to DNA damage, triggering the release of cytokines and growth factors, including IL-1, IL-4, IL-6, IL-13, and TGF-β. TGF-β activates Smad3, PI3K/AKT, and p38 MAPK pathways, promoting myofibroblast transdifferentiation. This model demonstrates alveolar damage, collagen accumulation, dyspnea, fatigue, and weight loss[24,25].

Gambir extract is a dried aqueous extract obtained from the sap of the leaves and young twigs of *Uncaria gambir* (Hunter) Roxb[26]. In this study, *U. Gambir* sap powder was used to obtain a purified semi-polar ethyl acetate extract isolate of *U. Gambir*.

The *U. gambir* nanoparticle formulation exhibited an average particle size of approximately 78 nm, demonstrated stability within a pH range of 3–11, and showed gradual thermal stability, with degradation and decomposition occurring at high temperatures. The entrapment efficiency of bioactive compounds was very high (>97%) with good loading capacity, and the release profile was pH-dependent, showing slower release under acidic conditions and increased release under neutral to alkaline pH[16].

BW is a common measure used to monitor the general health status of rats with bleomycin-induced lung injury[7,9,27]. Weight loss on day 9 reflects the acute toxicity phase, characterized by lung injury and systemic inflammation, whereas partial recovery by day 23 indicates post-acute physiological improvement. G-NPs administration did not significantly alter BW, which is consistent with reports indicating that bleomycin causes early weight loss due to inflammation, oxidative stress, and metabolic disturbances[17,28]. Gambir nanoparticles did not significantly affect weight changes, aligning with the bleomycin model's acute (days 0–7) and fibrotic (days 14–28) phases[29,30].

Digital pathology image analysis methods using whole slide images (WSIs) have been increasingly applied to reduce subjectivity in assessing fibrotic tissue components while generating continuous quantitative data[2,9]. In this study, WSIs were utilized to quantify interalveolar septal thickness and collagen percentage. Bleomycin significantly increased tissue injury and collagen accumulation, serving as key indicators of therapeutic efficacy. *Uncaria gambir* nanoparticles demonstrated a dose-dependent effect; 50 and 100 mg/kg BW showed limited protection, whereas 200 mg/kg BW reduced injury, improved histopathological scores, and decreased collagen deposition approaching the negative control group. In line with previous research, gambir (262 mg/kg BW) has been reported to suppress the inflammatory cytokines and profibrotic mediators, such as TIMP-1 and type I collagen, thereby inhibiting collagen accumulation and improving histopathological features[12]. Similarly, other studies have reported that catechin nanoparticles significantly reduced fibroblast proliferation and collagen production induced by silica in the pulmonary interstitial tissue based on morphometric observations[31].

Assessment using the modified Ashcroft scoring system[32,33] also demonstrated that the G-NPs at 200 mg/kg BW group had a significantly lower degree of fibrosis compared to the 50 mg/kg BW and 100 mg/kg BW doses. These findings indicate that the antifibrotic effect of G-NPs (200 mg/kg BW dose) reduces the degree of fibrosis compared to the negative control, indicating good therapeutic effectiveness at this dose. The previous study reported that histopathological evaluation showed improvement in gambir-treated groups, particularly at the 262 mg/kg BW dose, which exhibited a modified Ashcroft score of grade 3[12].

This study suggests that the anti-fibrotic effect of G-NPs increases in a dose-dependent manner. Administration of G-NPs at 200 mg/kg BW resulted in a significantly greater reduction in the degree of fibrosis with 50 and 100 mg/kg BW doses. This condition may be attributed to the antioxidant activity of gambir.

Phytochemical analysis has shown that the primary antioxidant compound in *Uncaria gambir* is catechin, which its the dominant secondary metabolite[13].

Gambir extract derived from the dried aqueous extract of the sap of leaves and young twigs of *Uncaria gambir* (Hunter) Roxb. contains 86.07–89.34% catechin, identified in the ethyl acetate extract of *U. gambir*.[16] Catechin is the most active polyphenolic compound in gambir leaves (*Uncaria gambir* Roxb) and has been extensively investigated for its antioxidant, antiproliferative, and antineoplastic activities[31].

The improvement in histopathological outcomes following catechin treatment may be attributed to its antioxidant activity, reflected in the enhancement of enzymatic antioxidants (superoxide dismutase, catalase, glutathione peroxidase, and glutathione reductase) and non-enzymatic antioxidants, including glutathione and vitamins C, E, and A,[34] as well as the reduction of lipid peroxidation markers such as malondialdehyde, 4-hydroxynonenal, and F2-isoprostanes[35]. Previous investigations demonstrated that intervention administered with a gambir nanoparticle formulation encapsulated in sodium alginate (G-NPs) at a dose of 200 mg/kg body weight significantly increased SOD levels to 13.69 ng/mL in cancer-model rats. Administration of nano-gambir (G-NPs) at a dose of 100 mg/kg body weight showed the best results in restoring catalase (CAT) enzyme levels to 7.18 ng/mL. In addition to these enzyme systems, therapy with G-NPs at a dose of 200 mg/kg body weight proved to be the most effective in maintaining non-enzymatic antioxidants such as glutathione (GSH) at a high level of 455.6 ng/mL[16].

These antioxidant effects may reduce lung tissue damage, edema, and fibrosis[34]. These results indicate that G-NPs induce histological improvement. This effect may be attributed to the ability of nanoparticles to maintain stability and bioactivity more effectively during oral administration[31]. The study results indicate that G-NPs exert antifibrotic effects against bleomycin-induced histopathological changes in the lungs, with the strongest effect observed at a dose of 200 mg/kg BW.

The present study is limited by its relatively short observation period and restricted range of evaluation methods. The short duration of treatment and follow-up period restricted the evaluation of long-term therapeutic efficacy and fibrosis reversibility. Treatment efficacy was assessed through histopathological analysis, without evaluating lung function, molecular biomarkers of fibrosis and inflammation, or cellular signaling mechanisms. In addition, no comparison was made with established antifibrotic drugs, such as Pirfenidone and Nintedanib. Furthermore, pharmacokinetic analysis, nanoparticle characterization, and systemic toxicity assessment were not performed. Future studies should incorporate longer observation periods, functional and molecular assessments, comparative analyses with standard antifibrotic therapies, and comprehensive investigations of nanoparticle pharmacokinetics. Nevertheless, this study assessed histopathological parameters involved in pulmonary fibrosis, including the percentage of lung injury, semi-quantitative lung injury score, interalveolar septal thickness, fibrosis score based on the modified Ashcroft scale, and collagen deposition percentage using H E and Masson's trichrome staining. Therefore, these findings provide a comprehensive histopathological assessment of the antifibrotic effects of G-NPs on pulmonary fibrosis.

5. CONCLUSIONS

Treatment with G-NPs in a bleomycin-induced rat model of pulmonary fibrosis resulted in a significant improvement in histopathological parameters, including percentage of lung injury, semi-quantitative injury scores, alveolar septal thickness, collagen deposition, and Ashcroft scores. Among the tested doses, the 200 mg/kg BW dose demonstrated the greatest efficacy, markedly reducing injury severity and collagen accumulation toward near-normal conditions, thereby suggesting strong antifibrotic potential. These results serve as a basis for future studies investigating the molecular mechanisms and potential clinical applications of G-NPs as an antifibrotic therapy.

6. ACKNOWLEDGEMENTS

The authors gratefully acknowledge Universitas Airlangga, through the Institute for Research and Community Service (LPPM), for providing research funding under the Airlangga Research Fund (ARF) Batch 1, specifically the "Master's Thesis Research" scheme in 2025, under Contract No. 1839/UN3.LPPM/PT.01.03/2025, dated March 4, 2025.

Author contribution

LNR: methodology, data collection and analysis, and manuscript preparation. GM: conceptualization, supervision, manuscript editing, and critical review. ASR, DF, and NSA: data analysis and validation, and manuscript review. ASS: methodology and histopathological diagnosis. HFT: histopathological diagnosis and statistical analysis. All authors: reviewed and approved the final manuscript. All authors reviewed, approved, and take responsibility for the final manuscript.

Funding

This study was funded by Universitas Airlangga through the LPPM under the Airlangga Research Fund Batch 1, "Penelitian Tesis Magister," (Contract: 1839/UN3.LPPM/PT.01.03/2025), dated March 4, 2025.

Conflict of interest
None to declare.

Ethics approval
All experimental procedures were carried out in accordance with the *Guide for the Care and Use of Laboratory Animals*. This study was approved by the Ethical Committee, Faculty of Veterinary Medicine, Universitas Airlangga (Approval No. 2.KEH.111.07.2025).

Article info*:*
Received May 22, 2026
Received in revised form August 29, 2026
Accepted October 6, 2026

REFERENCES

1. Caporarello N, Ligresti G. Vascular Contribution to lung Rrepair and fibrosis. Am J Respir Cell Mol Biol. 2023;69(2):135–46.
2. Lai R, Zhao C, Guo W, Xiao Y, Li R, Liu L, et al. The longitudinal and regional analysis of bleomycin-induced pulmonary fibrosis in mice by microcomputed tomography. Heliyon. 2023;9(5):e15681.
3. Bale LK, West SA, Oxvig C, Andersen KS, Roden AC, Haak AJ, et al. Genetic and pharmacological inhibition of PAPP-A reduces bleomycin-induced pulmonary fibrosis in aged mice via reduced igf signaling. Aging Biol. 2024;1(1):20240023.
4. B. Moore B, Lawson WE, Oury TD, Sisson TH, Raghavendran K, Hogaboam CM. Animal models of fibrotic lung disease. Am J Respir Cell Mol Biol. 2013;49(2):167–79.
5. Wang J, Li K, Hao D, Li X, Zhu Y, Yu H, et al. Pulmonary fibrosis: pathogenesis and therapeutic strategies. MedComm (2020). 2024;5(10):e744.
6. Araldi GL, Hwang YW, Raghu G. Development and evaluation of ABI-171, a new fluoro-catechin derivative, for the treatment of idiopathic pulmonary fibrosis. Int J Mol Sci. 2024;25(21):11827.
7. Yang X, Huang XJ, Chen Z, Xu AL, Zhou H, Bi XL, et al. A novel quantification method of lung fibrosis based on Micro-CT images developed with the optimized pulmonary fibrosis mice model induced by bleomycin. Heliyon. 2023;9(3):e13598.
8. Muri J, Durcová B, Slivka R, Vrbenská A, Makovická M, Makovický P, et al. Idiopathic pulmonary fibrosis: Review of current knowledge. Physiol Res. 2024;73(4):487-97.
9. Van Heest A, Wang Y, Zhang L, Phillips LA, Karsen SD, Nelson C, et al. Quantitative assessment of pulmonary fibrosis in a murine model via a multimodal imaging workflow. Chem Biomed Imaging. 2025;3(2):85–94.
10. Jusman SWA, Amalia MF, Paramita R, Ningsih S, Fadilah F. Structure-based screening of inhibitor platelet-derived growth factor from ethanol extract of *Uncaria gambir* (Hunter) Roxb. as an antifibrotic in keloid fibroblast cells. J Appl Pharm Sci. 2023;13(03):036–043.
11. Ningsih SS, Fadilah F, Jusman SWA, Syaidah R, Yashiro T. Profibrotic inflammatory cytokines and growth factors are predicted as the key targets of *Uncaria gambir* (Hunter) roxb. in keloids: An epistatic and molecular simulation approach. Pharmaceuticals. 2024;17(6):662.
12. Desdiani D, Rengganis I, Djauzi S, Setiyono A, Sadikin M, Jusman SWA, et al. Fibropreventive and antifibrotic effects of *Uncaria gambir* on rats with pulmonary fibrosis. Evid Based Complement Alternat Med. 2022; 2022:6721958.
13. Shiyan S, Safitri IN, Nathasia J, Fitrotunnisa L, Fransiska OL, Salsabillah T, et al. FTIR spectroscopy combined with chemometrics for evaluation of Gambir Extract – self nano emulsifying formulation from *Uncaria gambir* Roxb. Biointerface Res Appl Chem. 2022;13(2):153.
14. Pramanik F, Satari MH, Azhari A. Cytotoxic *Act*ivity of Gambier Leave (*Uncaria gambir*) ethyl acetate extract on mouse embryonic fibroblast cell (NIH-3T3) using MTT assay. Open Dent J. 2023;17(1):e187421062212300.
15. Deng Z, Kalin GT, Shi D, Kalinichenko VV. Nanoparticle delivery systems with cell-specific targeting for pulmonary diseases. Am J Respir Cell Mol Biol. 2021;64(3):292-307.
16. Wardana AP, Aminah NS, Kristanti AN, Fahmi MZ, Zahrah HI, Widiyastuti W, et al. Nano *Uncaria gambir* as chemopreventive agent against breast cancer. Int J Nanomedicine. 2023;18:4471-84.
17. Dik WA, McAnulty RJ, Versnel MA, Naber BAE, Zimmermann LJI, Laurent GJ, et al. Short course dexamethasone treatment following injury inhibits bleomycin induced fibrosis in rats. Thorax. 2003;58(9):765-71.
18. Bankhead P, Loughrey MB, Fernández JA, Dombrowski Y, McArt DG, Dunne PD, et al. QuPath: Open source software for digital pathology image analysis. Sci Rep. 2017;7(1):16878.
19. Humphries MP, Maxwell P, Salto-Tellez M. QuPath: The global impact of an open source digital pathology system. Comput Struct Biotechnol J. 2021;19:852-9.
20. Cui P, Tang Z, Zhan Q, Deng C, Lai Y, Zhu F, et al. *In vitro* and vivo study of tranilast protects from acute respiratory distress syndrome and early pulmonary fibrosis induced by smoke inhalation. Burns. 2022;48(4):880-895.
21. Liu ZW, M.Y. Zhao, Su XL, Ye TH, Y.J. Zhuang, Y. Zhang, et al. The antifibrotic effect and mechanism of a novel tyrosine kinase inhibitor, ZSP1603, in preclinical models of pulmonary fibrosis. Eur Rev Med Pharmacol Sci. 2020;24(3):1481-91.
22. Lumanto P, Macparland S, Nakib D. QuPath Stain quantification of whole tissue by percent area v1. https://dx.doi.org/10.17504/protocols.io.6qpvrw64olmk/v1; 2025 [accessed 13 February 2026].
23. Holm PH, Olsen KB, De Mets RDM, Banner J. Quantifying cardiac tissue composition using qupath and cellpose: An accessible approach to postmortem diagnosis. Lab Invest. 2025;105(1):102181.
24. Ju N, Hayashi H, Shimamura M, Baba S, Yoshida S, Morishita R, et al. Prevention of bleomycin-induced pulmonary fibrosis by a RANKL peptide in mice. Sci Rep. 2022;12(1):12474.
25. Ishida Y, Kuninaka Y, Mukaida N, Kondo T. Immune mechanisms of pulmonary fibrosis with bleomycin. Int J Mol Sci. 2023;24(4):3149.
26. Zhang L, Liu Z, Hu Y, Liu X, Yang Z, Liu Y, et al. Oleuropein ameliorates bleomycin-induced pulmonary fibrosis in mice by targeting TGF-β1 signaling pathway. Biomolecules. 2025;15(9):1211. https://doi.org/10.3390/biom15091211.
27. Taniguchi S, Kuroda K, Doi K ichi, Tanabe M, Shibata T, Yoshida T, et al. Revised structures of gambiriins A1, A2, B1, and B2, chalcane-flavan dimers from Gambir (*Uncaria gambir* Extract). Chem Pharm Bull (Tokyo). 2007;55(2):268-272.
28. Chen L, Zhao W. Apigenin protects against bleomycin-induced lung fibrosis in rats. Exp Ther Med. 2016;11(1):230-4.
29. Bonatti M, Pitozzi V, Caruso P, Pontis S, Pittelli MG, Frati C, et al. Time-course transcriptome analysis of a double challenge bleomycin-induced lung fibrosis rat model uncovers ECM homoeostasis-related translationally relevant genes. BMJ Open Respir Res 2023;10(1):e001476.
30. Tukhovskaya EA, Palikova YA, Severyukhina MS, Ismailova AM, Palikov V, Slashcheva GA, et al. Different degrees of expression of pulmonary fibrosis signs with intratracheal administration of bleomycin at different doses in male SD rats (a study aimed at helping to select the optimal bleomycin

dose for modeling pulmonary fibrosis). Front Pharmacol. 2025;16:1702991.
31. Yao JJ, Ma QQ, Shen WW, Li LC, Hu D. Nano-enabled delivery of EGCG ameliorates silica-induced pulmonary fibrosis in rats. Toxicology. 2022;469:153114.
32. Cox BP, Hannan RT, Batrash N, Raichura P, Sperling AI, Shim YM, et al. Local, Quantitative morphometry of fibroproliferative lung injury using laminin. Am J Respir Cell Mol Biol. 2024;71(1):23-29.
33. Testa LC, Jule Y, Lundh L, Bertotti K, Merideth MA, O'Brien KJ, et al. Automated digital quantification of pulmonary fibrosis in human histopathology specimens. Front Med. 2021;8:607720.
34. Mokra D, Adamcakova J, Mokry J. Green tea polyphenol (-)-epigallocatechin-3-gallate (EGCG): A time for a new player in the treatment of respiratory diseases? Antioxidants. 2022;11(8):1566.
35. Sheng Y, Sun Y, Tang Y, Yu Y, Wang J, Zheng F, et al. Catechins: Protective mechanism of antioxidant stress in atherosclerosis. Front Pharmacol. 2023;14:1144878.